BULLETIN OF THE POLISH ACADEMY OF SCIENCES
TECHNICAL SCIENCES, Vol. 72(5), 2024, Article number: e1511046
DOI: 10.24425/bpasts.2024.1511046

A high-accuracy Stewart–lift platform based on a programmable logic controller – comparative case studies

Dawid PAWUŚ[1]*, Michał WITEK[2], Łukasz KLAR[2], and Krzysztof BOCHENEK[2]

[1] Faculty of Electrical Engineerig, Automatic Control and Informatics, Opole University of Technology, Prószkowska Street 76, Opole, 45-758, Poland

[1] KBA Automatic Sp. z o.o., Technologiczna Street 2A, Opole, 45–839, Poland

Abstract. The study reports the results of a comparative analysis of advanced high-accuracy Stewart-lift platform along with a comparative study of dynamic control. A control system powered by a programmable logic controller (PLC) was used. The properties of the system were described using a dynamic model using the Lagrange method. The real object was verified by performing several tests and comparing them using quality indicators. The results of verification tests conclusively demonstrate the system suitability for applications within industrial automation and robotics systems.

Keywords: Stewart–lift platform; inverse dynamics method; robust control; practical verification; comparative studies.

SYMBOLS

A1, A2, A3	points of the platform transmission shaft
B1, B2, B3	characteristic points of attachment
C1, C2, C3	characteristic points of the platform
D_w, D_R	coefficients of viscous friction
$\mathbf{I}$	the identity matrix
J	moment of inertia
L	length of each connecting rods
M_{01}, M_{02}, M_{03}	resistive moments resulting from friction
$\tilde{P}_\varphi, \tilde{P}_\vartheta, \tilde{P}_{h_0}$	external forces of the relevant variables
$\mathbf{Q}$	the symmetric, positive definite $n \times n$-matrix
R	length of each arm
$\mathbf{T}_r, T_{s1}, T_{s2}, T_{s3}$	motor torques
T, U	kinetic and potential energy, respectively
a, c	an equilateral triangle resulting distances
b	half distance between the mounting points
$\vec{g}$	gravity acceleration
k_p	gear ratio
m_L	mass of the load
m_l	mass of the platform arms
m_r	mass of the transmission arms
m_t	mass of the platform
q_1, q_2, q_3	joint variables
x_{C1}, y_{C1}, z_{C1}	coordinates of the point (for example for C1)
α	coefficient satisfying the $0 < \alpha < 1$
$\delta A q_k$	virtual work performed on the platform system by external and friction forces
φ, ϑ, h_0	platform external coordinates
φ_i, φ_f	the initial and final value (for example for φ)
$\eta, \overline{\eta}$	gear efficiency and uncertainty, respectively
$\frac{\partial}{\partial x}$	example symbol of differentiate
$\frac{d}{dt}, (\dot{.})$	symbols of derivative
$(\ddot{.})$	second derivative symbol
$(\hat{.}), \|.\|$	estimation and norm operator, respectively
u, v, w	$u = \cos(q_1)$, $v = \cos(q_2)$, $w = \cos(q_3)$, the variables are explained in article [1]
V	motor speed before the transmission

1. INTRODUCTION

This paper continues the research on the Stewart platform, expanding upon the previously studied 3-RSS configuration [1]. Building on earlier findings, we further investigate the platform capabilities and its potential applications in industrial automation and robotics systems. Building upon the previous work, a deeper comparative analysis of dynamic control and system properties is conducted to further validate applicability in industrial automation and robotics systems.

Parallel manipulators, often referred to as parallel robots, are experiencing an increasing range of application across a wide variety of industries and scientific disciplines. In the modern control theory and practice dedicated to the robotic tasks, the Stewart platform is gaining more applicable interest. These studies include problems related to control and stabilization [2–4], vibration isolation and energy harvesting [5–7] or development and technical applications [8]. Other research concerns modeling and theory [9, 10], as well as robotics and dynamic formu-

*e-mail: dawid.pawus@student.po.edu.pl

Manuscript submitted 2024-02-04, revised 2024-06-04, initially accepted for publication 2024-06-27, published in September 2024.

lations [11, 12]. New solutions based on variety of construction structure can be found in real-life assignments [13, 14].

A new approach seems to include solutions implementing artificial intelligence (AI) in addition to the existing object layer, either in the real-life objects or the Stewart platform simulation model. An example is [15] where authors introduce a generalizable robust control technique for parallel manipulator. Based on the time-delay linear quadratic integral controller (LQI) the on-line artificial neural network (ANN) is used as a adjuster for the gain of the cost function. This hybrid connection creates a synergy towards minimization the real-time tracking error of nonlinear and large time-delay systems. This has been confirmed by simulation studies.

The study in [16] appears to be similar to the previously presented idea. In this assignment authors present the control of a nonlinear Stewart platform and put more emphasis on artificial intelligence algorithms. Using deep reinforcement learning (DRL), they considered three learning algorithms: the deep deterministic policy gradient (DDPG), the proximal policy optimization (PPO) and the asynchronous advantage actor–critic (A3C) in order to obtain appropriate control parameters. The received satisfactory control performance has been confirmed only in simulation manner.

Interesting research results were also obtained in many other studies. Thus, the research effectively addresses the issues related to inverse kinematics and Stewart platform design [17–19], kinematic analysis and applications of Stewart platforms [20,21] or motion cueing algorithms and Stewart platform applications [22–24].

An illustrative instance within the context of the discussed field can be found in the paper [8]. This publication introduces an isotropic Stewart configuration, outlining the structure design and the construction of an experimental prototype of the platform. To assess the isotropic properties, the paper conducts verification experiments grounded in static principles. Furthermore, the paper develops and scrutinizes a model pertaining to the isotropic dynamics of the Stewart platform.

In the paper [25], researchers delve into the dynamics and control of a six-axis vibro-isolator using a flexible Stewart platform. Meanwhile, the manuscript [26] introduces a novel dynamic model for the Stewart platform featuring flexible hinges, employing the complex Kane equation along with the principle of virtual forces.

The study in [27] offers remarkable results, as it provides a detailed examination of a Stewart platform designed for generating six degrees of freedom spatial orbits. Within this research, the authors explore the use of spatial orbits as a means to test MEMS inclinometers. The paper delves into the analysis of inverse and forward kinematics for the purpose of controlling and measuring the robot position and orientation. The platform is manipulated to produce conical motion, enabling the determination of sensitivities for the gyroscope, accelerometer, and tilt sensor.

Other important issues discussed in this article, regarding drives [28–30], actuators [31], sensors [32, 33] and encoders [34], are also presented in scientific works.

In this manuscript, we continue the previous research from [1], expanding the current state of knowledge. The scope of work in this work is focused on checking the capabilities of the Stewart platform technology and comparative studies of various variants of its operation.

In many industrial tasks, elevators, lifts and other components must be reliable, accurate and fast. We thus present verification of the project tests and recall the design of the Steward platform prototype. Naturally, we also take into account complex research problems and various system control scenarios.

The structure of the article is as follows. After an introduction to examples of the application of the proposed solution in Section 1, a detailed description and representation of the tested system was made, along with dynamic equations in Section 2. Then, the real-life Stewart-lift platform and its digital twin were presented. This chapter describes the hardware and software parts. Section 4 presents quality indicators and then conducts a comparative study consisting of three sets of extensive tests. The article ends with conclusions.

2. CONTRIBUTIONS

In this paper, we have extended the research on the Stewart platform, particularly focusing on its application as a real-world elevator system. The main contributions of this work can be summarized in several aspects.

Extensive comparative research was conducted on the real-life Stewart platform, consisting of six comprehensive tests under different scenarios and load conditions. This research aimed to evaluate the platform performance and behavior under various parameters, such as velocity, torque, and power.

The developed dynamic model was experimentally validated through extensive tests on the real-life Stewart platform. The experimental results confirmed the accuracy and reliability of the proposed model in predicting the platform behavior.

The findings from this research provide valuable insights into the capabilities and potential applications of the Stewart platform in industrial automation, robotics, and precision tasks.

3. SYSTEM REPRESENTATION

Crafting a precise description of the envisioned system represents a crucial initial stride in the development of a Stewart platform model – a highly precise real-world elevator system. These platforms hold indispensable significance in the automation industry, primarily due to their exceptional and coveted attributes.

The following subsections will be an introduction to the system design methodology, its mathematical equations and related aspects.

3.1. Details and description of the tested Stewart platform

A fundamental assumption in our model is the fixed orientation of the platform top, which prohibits any rotation around the z-axis (referred to as *Yaw* rotation). To achieve this, we employ ‘ball’ connections at the tips of the power system rods,

introducing two Degrees of Freedom (2 DoFs) for each connection. While this approach presents challenges in the modeling process, it conforms with our objective of simulating a Stewart platform functioning as an elevator system while adhering to these specific constraints [1, 35].

We have made specific assumptions regarding the system mass distribution. The platform itself is characterized by a mass of 30 kg, while the rods connecting the drive system's tips to the platform weigh 5 kg, and the reinforced arms stemming from the gears contribute an additional 10 kg. The height to which the elevator must lift determines the parameters of both the drive system arms and the length of the rods linking the motion system to the platform. To simplify the modeling process, we have defined key points within the system (as illustrated in Fig. 1):

- Points labeled with C represent the characteristic points of the platform, and their coordinates are denoted as x, y, and z.
- B designates the attachment points of the drive system arms.
- A denotes the central points of the transmission shaft connected to the drive system arms [1, 35].

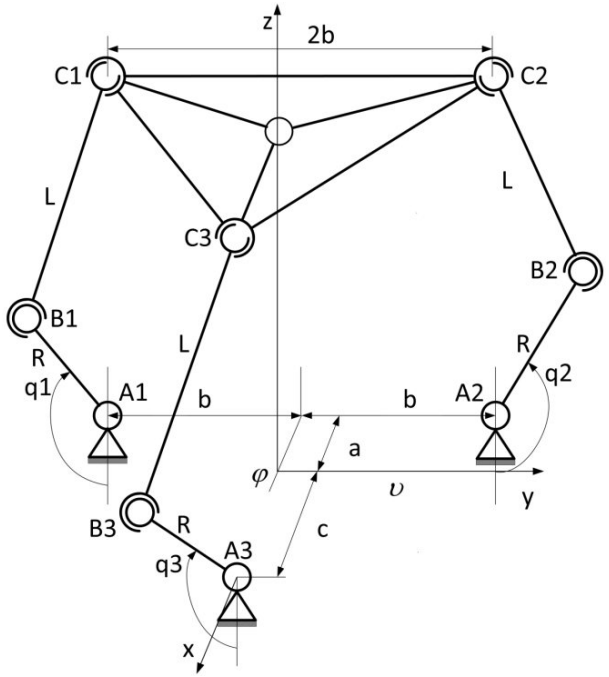

Fig. 1. The scheme of the Stewart platform [1, 35]

It was assumed that the elevator would be able to lift a load of 100 kg to a height of 425.5 mm. The maximum range of movement of the platform was measured using a cable encoder mounted on the platform and the result was 4255 units, which is 425.5 mm. Considering the critical need for accurate movement and the imperative to minimize dynamic platform deviations, it is essential to acknowledge that the drive system is inherently non-synchronous owing to its intricate structure.

The drive system comprises frequency inverters, three-phase servomotors (in certain instances, induction motors with specialized capabilities), as well as gears tailored to these servomotors [35].

The drive armatures rotate around an axis that runs through the very heart of the gear shaft. For the A3 point, this axis aligns itself parallel to the system y-axis. In contrast, the remaining rotational axes are offset by either 120 or 240 degrees. The parameters q_1, q_2, and q_3, as illustrated in Fig. 1, represent the angular orientations of the arms affixed to the transmission mechanism [35].

R corresponds to the length of the arms, while L represents the length of the connecting rods that link the tips of the drive arms to the attachment points on the platform. Variable b denotes half the distance between these platform attachment points, with the distance between any pair of platform points being equal. Additionally, a and c denote the distances resulting from the equilateral triangle positioning of C1, C2, and C3 points [35].

With this particular platform design, the focal point of the equilateral triangle, highlighted in Fig. 1 by a circle connected to the arms, is subjected to vertical motion only. Its initial height concerning the global coordinate system x, y, z is represented as h_0 [35].

The axis aligning with the x direction, positioned at h_0, serves as the rotational axis for the platform model, with φ representing the coordinate of this rotation. Furthermore, the platform undergoes rotation around the axis parallel to the y direction at h_0, governed by ϑ [35].

The mass of the platform is marked as m_t and the masses of the arms connected to the transmission as m_r. Additionally, our modeling takes into account an extra mass located on the platform, referred to as m_L. Given that, this mass may be positioned off-center from the platform center, the model accommodates shifts along three axes in the center of mass of the load and the consequent alterations in the load moments of inertia with regard to the coordinate system axis [35].

The next subsection will effectively discuss the dynamics model of the discussed object.

3.2. Dynamic model of the analysed Stewart platform

First, we consider the dependence of the rotational velocities of the arms attached to the gear and the velocities of variables φ, ϑ and h_0. Given these provisions, we have the following calculations:

$$\begin{bmatrix} \frac{dq_1}{dt} \\ \frac{dq_2}{dt} \\ \frac{dq_3}{dt} \end{bmatrix} = \mathbf{I}_{3\times 3} \begin{bmatrix} \frac{-1}{\sqrt{1-u^2}} \\ \frac{-1}{\sqrt{1-v^2}} \\ \frac{-1}{\sqrt{1-w^2}} \end{bmatrix}^T \begin{bmatrix} q_{11t} & q_{12t} & q_{13t} \\ q_{21t} & q_{22t} & q_{23t} \\ q_{31t} & q_{32t} & q_{33t} \end{bmatrix} \begin{bmatrix} \frac{d\varphi}{dt} \\ \frac{d\vartheta}{dt} \\ \frac{dh_0}{dt} \end{bmatrix}, \quad (1)$$

where $\mathbf{I}_{3\times 3}$ stands for the 3×3 identity matrix and coefficients q_{nkt} $(n, k = 1, 2, 3)$ have been shown in equation (2) [1, 35].

$$\begin{bmatrix} q_{11t} & q_{12t} & q_{13t} \\ q_{21t} & q_{22t} & q_{23t} \\ q_{31t} & q_{32t} & q_{33t} \end{bmatrix} =$$

$$\begin{bmatrix} \frac{\partial u}{\partial x_{C1}}\frac{\partial x_{C1}}{\partial \varphi}+\frac{\partial u}{\partial y_{C1}}\frac{\partial y_{C1}}{\partial \varphi}+\frac{\partial u}{\partial z_{C1}}\frac{\partial z_{C1}}{\partial \varphi} & \dots \\ \frac{\partial v}{\partial x_{C1}}\frac{\partial x_{C1}}{\partial \varphi}+\frac{\partial v}{\partial y_{C1}}\frac{\partial y_{C1}}{\partial \varphi}+\frac{\partial v}{\partial z_{C1}}\frac{\partial z_{C1}}{\partial \varphi} & \dots \\ \frac{\partial w}{\partial x_{C1}}\frac{\partial x_{C1}}{\partial \varphi}+\frac{\partial w}{\partial y_{C1}}\frac{\partial y_{C1}}{\partial \varphi}+\frac{\partial w}{\partial z_{C1}}\frac{\partial z_{C1}}{\partial \varphi} & \dots \end{bmatrix}$$

$$\begin{bmatrix} \dots & \frac{\partial u}{\partial x_{C1}}\frac{\partial x_{C1}}{\partial \vartheta}+\frac{\partial u}{\partial y_{C1}}\frac{\partial y_{C1}}{\partial \vartheta}+\frac{\partial u}{\partial z_{C1}}\frac{\partial z_{C1}}{\partial \vartheta} & \dots \\ \dots & \frac{\partial v}{\partial x_{C1}}\frac{\partial x_{C1}}{\partial \vartheta}+\frac{\partial v}{\partial y_{C1}}\frac{\partial y_{C1}}{\partial \vartheta}+\frac{\partial v}{\partial z_{C1}}\frac{\partial z_{C1}}{\partial \vartheta} & \dots \\ \dots & \frac{\partial w}{\partial x_{C1}}\frac{\partial x_{C1}}{\partial \vartheta}+\frac{\partial w}{\partial y_{C1}}\frac{\partial y_{C1}}{\partial \vartheta}+\frac{\partial w}{\partial z_{C1}}\frac{\partial z_{C1}}{\partial \vartheta} & \dots \end{bmatrix}$$

$$\begin{bmatrix} \dots & \frac{\partial u}{\partial x_{C1}}\frac{\partial x_{C1}}{\partial h_0}+\frac{\partial u}{\partial y_{C1}}\frac{\partial y_{C1}}{\partial h_0}+\frac{\partial u}{\partial z_{C1}}\frac{\partial z_{C1}}{\partial h_0} \\ \dots & \frac{\partial v}{\partial x_{C1}}\frac{\partial x_{C1}}{\partial h_0}+\frac{\partial v}{\partial y_{C1}}\frac{\partial y_{C1}}{\partial h_0}+\frac{\partial v}{\partial z_{C1}}\frac{\partial z_{C1}}{\partial h_0} \\ \dots & \frac{\partial w}{\partial x_{C1}}\frac{\partial x_{C1}}{\partial h_0}+\frac{\partial w}{\partial y_{C1}}\frac{\partial y_{C1}}{\partial h_0}+\frac{\partial w}{\partial z_{C1}}\frac{\partial z_{C1}}{\partial h_0} \end{bmatrix}. \quad (2)$$

In our research studies we consider our own model determined using Lagrange equations [28, 35].

In our considerations, we will mention the key part of the calculations, which is the virtual work performed on the platform system by external forces and friction forces. The following patterns were used [35]:

$$M_1 = \left(T_{s1}k_p\eta - M_{01}(\dot{q}_1,t)\right)\left(\frac{-1}{\sqrt{1-u^2}}\right) - \left(D_w k_p^2 + D_R\right)\frac{1}{1-u^2}\left(q_{11t}\dot{\varphi} + q_{12t}\dot{\vartheta} + q_{13t}\dot{h}_0\right), \quad (3)$$

$$M_2 = \left(T_{s2}k_p\eta - M_{02}(\dot{q}_2,t)\right)\left(\frac{-1}{\sqrt{1-v^2}}\right) - \left(D_w k_p^2 + D_R\right)\frac{1}{1-v^2}\left(q_{21t}\dot{\varphi} + q_{22t}\dot{\vartheta} + q_{23t}\dot{h}_0\right), \quad (4)$$

and

$$M_3 = \left(T_{s3}k_p\eta - M_{03}(\dot{q}_3,t)\right)\left(\frac{-1}{\sqrt{1-w^2}}\right) - \left(D_w k_p^2 + D_R\right)\frac{1}{1-w^2}\left(q_{31t}\dot{\varphi} + q_{32t}\dot{\vartheta} + q_{33t}\dot{h}_0\right), \quad (5)$$

where T_{s1}, T_{s2} and T_{s3} are the motor torques, M_{01}, M_{02} and M_{03} are the resistance torques resulting from friction (it decreases to zero shortly after the start of movement). The variables D_w and D_R are the viscous friction coefficients, and k_p is the gear ratio (determines the velocity ratio on the primary gear and the secondary sides of the gear). In turn, η is the efficiency of the transmission, which generally depends on the engine velocity. Taking into account the gear efficiency is a fact worth emphasizing, because this coefficient has a huge impact on the control tasks. When we consider equations (3)–(5), we can note that the external forces affecting the system are as follows:

$$\tilde{P}_\varphi = M_1 q_{11t} + M_2 q_{21t} + M_3 q_{31t} - D_\varphi \dot{\varphi}, \quad (6)$$

$$\tilde{P}_\vartheta = M_1 q_{12t} + M_2 q_{22t} + M_3 q_{32t} - D_\vartheta \dot{\vartheta}, \quad (7)$$

and

$$\tilde{P}_{h_0} = M_1 q_{13t} + M_2 q_{23t} + M_3 q_{33t} - D_{h_0}\dot{h}_0. \quad (8)$$

Equations (6)–(8) are used to determine the required motor torques. They also enable the implementation of a given trajectory using inverse dynamics. For these equations, D_φ, D_ϑ, D_{h_0} are defined as the friction coefficients for a specific coordinate. In the complex model under consideration, controlling the inverse dynamics requires a very efficient computer that can carry out the model identification process and accurately select the controller settings. Nevertheless, this method is more accurate compared to, for example, the inverse kinematics method.

From the theoretical assumptions, discussions and calculations we will now move on to the next section. It will present the real-life Stewart-lift platform and its digital twin.

4. REAL-LIFE STEWART-LIFT PLATFORM AND ITS DIGITAL TWIN

This section will contain various graphics, as well as a detailed description of the physical implementation of the object, from the hardware part to the software part. Moreover, it also includes device diagrams, 3D graphics of the object and images of the real object.

4.1. Hardware part – description, elements and real-life object

The real-life object has been built based on the design plan (see Fig. 2) through the 3D model (see Fig. 3) to the final object (see Fig. 4).

Moreover, in order to maintain correct control process, a digital twin has been made, which provides a solid support especially in industrial tasks (see Fig. 5).

The CAD model was created in the Fusion360 environment (Autodesk). Then it was imported into the NX MCD environment (Siemens), where connectors, drives and issues related to kinematics were created. The PLC controller along with the calculations and its communication side were simulated in PLCSIM Advanced (Siemens), and the SIMIT environment (Siemens) was used to simulate network communication with the drives. Thanks to this solution, the entire system was transferred to the digital world.

The height of the platform was measured using a LIKA SFA-1000-GA-1000-M2 cable encoder, the resolution of which is 0.1 mm. It is connected directly to the PLC controller via the TM PosInput module (catalog number 6ES7551-1AB00-0AB0). Communication between the encoder and the PLC takes

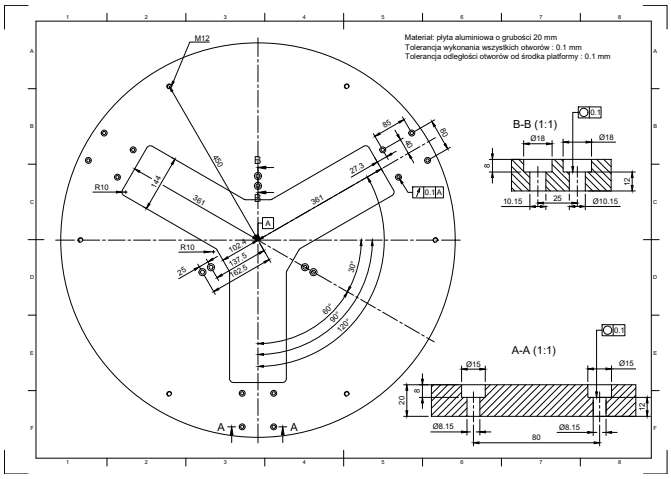

Fig. 2. The fragment of plans for the developed Stewart-lift platform [source: authors]

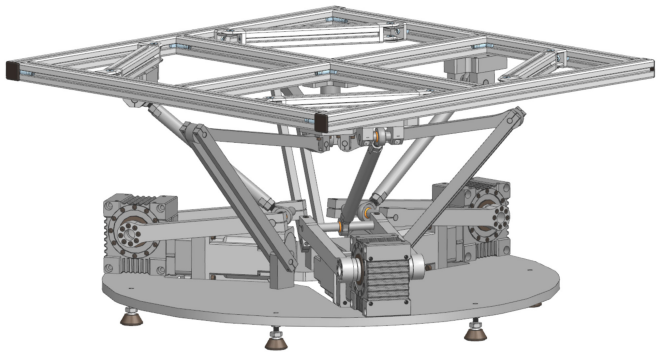

Fig. 3. View of the 3D model of the Stewart-lift platform [source: authors]

Fig. 4. The real-life Stewart-lift platform [source: authors]

place using the SSI protocol. Thanks to this hardware configuration, we were able to collect position data and display it directly in the TIA Portal. The position of the motor shafts was measured by encoders placed on the motor shafts (Siemens AM22DQC 4096). Other quantities, such as the platform deflection, were calculated (see Fig. 5).

Fig. 5. The real-life object and its digital twin [36]

The project was based on a very popular industrial programmable controller. This is an understandable and convenient solution due to the limitation of computing power and facilitates the implementation of the system. We also selected other modules for the control process (see Table 1).

Table 1
The list of devices/modules used in the Stewart platform

No.	Object	Model
1	PLC	Siemens S7-1500 (model CPU 1511TF-1 PN)
2	Servo drive	Siemens SIMOTICS 1FK2106-3AF00-0MA0
3	Absolute encoder	Siemens multiturn AM22DQC 4096
4	Inverters	Siemens SINAMICS 6SL3210-5HE15-0UF0
5	Gears	Atlanta Pivexin 98 03 050

Fig. 6. Control and executive elements of the platform [36]

Figure 6 shows a view of the system control cabinet and a set of actuators and drives.

The next subsection will describe the software part of the project.

4.2. Software part – description and components

In addition to the hardware part, the software layer is equally important. As a result of its development, it is possible to control and manage the entire operating process of the device. The result of comprehensive work on the real system, in parallel with the devices, was a software layer that was created for management and control tasks. First, it was decided to implement the theoretical results in the TIA Portal software. Next, an HMI panel with servo motor control was prepared to ensure the desired system performance (Fig. 7 and 8).

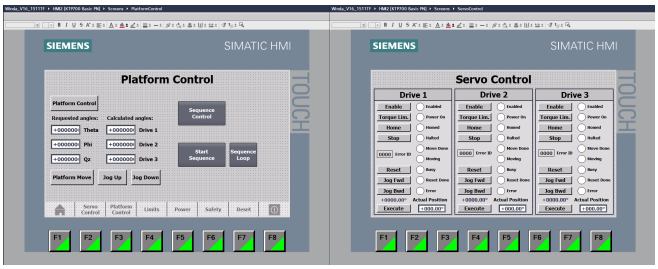

Fig. 7. The HMI screens in the development environment [36]

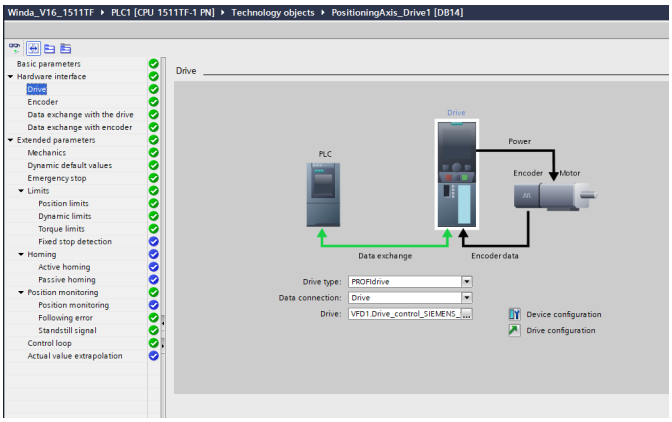

Fig. 8. The configuration of the servomotors [36]

In the following sections of the article, we will present the used quality indicators, and then we will move on to several verification tests.

5. QUALITY INDICATORS

Simulation tests of the control of the analyzed facility and practical verification were carried out using the following quality indicators [30, 37]:

- ISE – *integral of squared error* defined by

$$ISE = \int_{t_0}^{t} e^2(t)\,\mathrm{d}t, \tag{9}$$

where $e(t)$ is a control error.

- MOE – *minimum of energy* which is a integral of squared control signal

$$J(u_{MOE}) = \int_{t_0}^{t} u_{MOE}^2(t)\,\mathrm{d}t, \tag{10}$$

where u_{MOE} is the variable subject to the energy minimum test.

The presented indexes are integral, therefore they are sufficient to verify the control cases of analyzed approaches in the discussed tests.

The next chapter contains a set of tests conducted by the research team and the results obtained as a result of the research.

6. COMPARATIVE RESEARCH OF THE REAL-LIFE STEWART PLATFORM

This section presents a set of 6 extensive research tests that take into account a number of different scenarios and variants. This is to check the functioning of the platform as best as possible.

All 6 tests can be divided into 3 main comparative tests. Figures 9 and 10 are related to Tables 2 and 3, which means that they represent the first stage of the experiments. The next experiment is shown in Figures 11 with 12, and also Tables 4 together with 5 present comparative results for these cases. Next, Figs. 13 and 14 and Tables 6 as well as 7 show the results for the third and final comparative study.

The first study involved examining the motion properties of the platform in the absence of a load. The movement was made from a level of 10 mm to 250 mm. The assumed variable values were $\phi = 0$ rad and $\vartheta = 0$ rad. Three different velocities are included as the reference to the inverter, with $V_1 < V_2 < V_3$. Velocity [rpm], actual torque [Nm], actual power [kW] were measured for each velocity V. The graphical results of this stage of research are presented in Fig. 9. The measured quality indicators are included for this study in Table 2.

The first study involved examining the motion properties of the platform in the absence of a load. The platform movement was tested from a level of 10 mm to 250 mm. The controlled variables were set to $\phi = 0$ rad and $\vartheta = 0$ rad. Three different velocities of the platform movement, denoted as $V_1 < V_2 < V_3$, were used as reference inputs to the inverter. For each velocity, the rotational speed of the motors (velocity [rpm]), actual torque (actual torque [Nm]), and actual power (actual power [kW]) were measured. Velocity measurement is made by an encoder mounted on the motor shaft (Siemens AM22DQC 4096). The graphical results of this study are presented in Fig. 9, and the corresponding quality indicators are listed in Table 2.

This stage of research is complemented by the stage of testing the movement properties of the platform in the return movement, i.e. from 250 mm to 10 mm. The methodology of these tests in the second study is consistent with the first study. The same variable names were adopted, as well as three different variable values from V_1 to V_3. Again, each velocity V was measured for velocity [rpm], actual torque [Nm] and actual power [kW]. Figure 10 and Table 3 represent the results of this research.

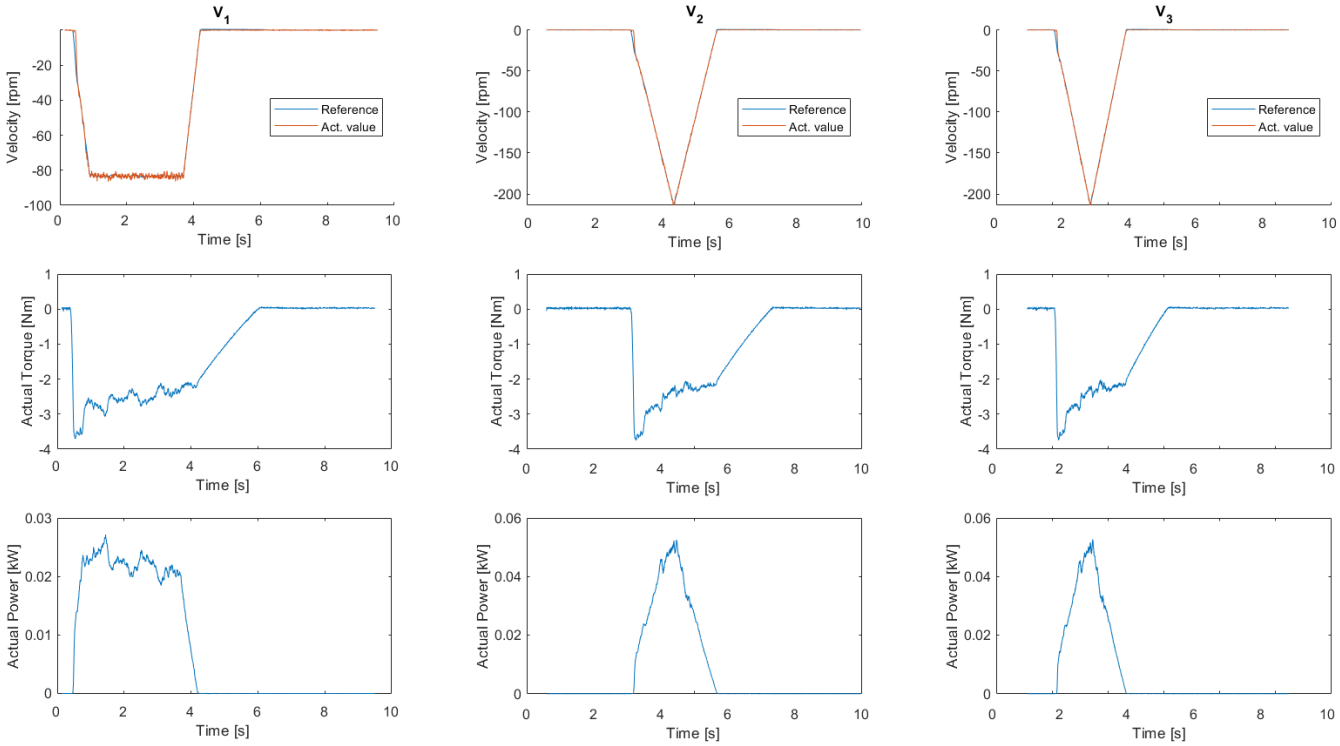

Fig. 9. Test 1. Platform unloaded – movement 10 to 250 mm [source: authors]

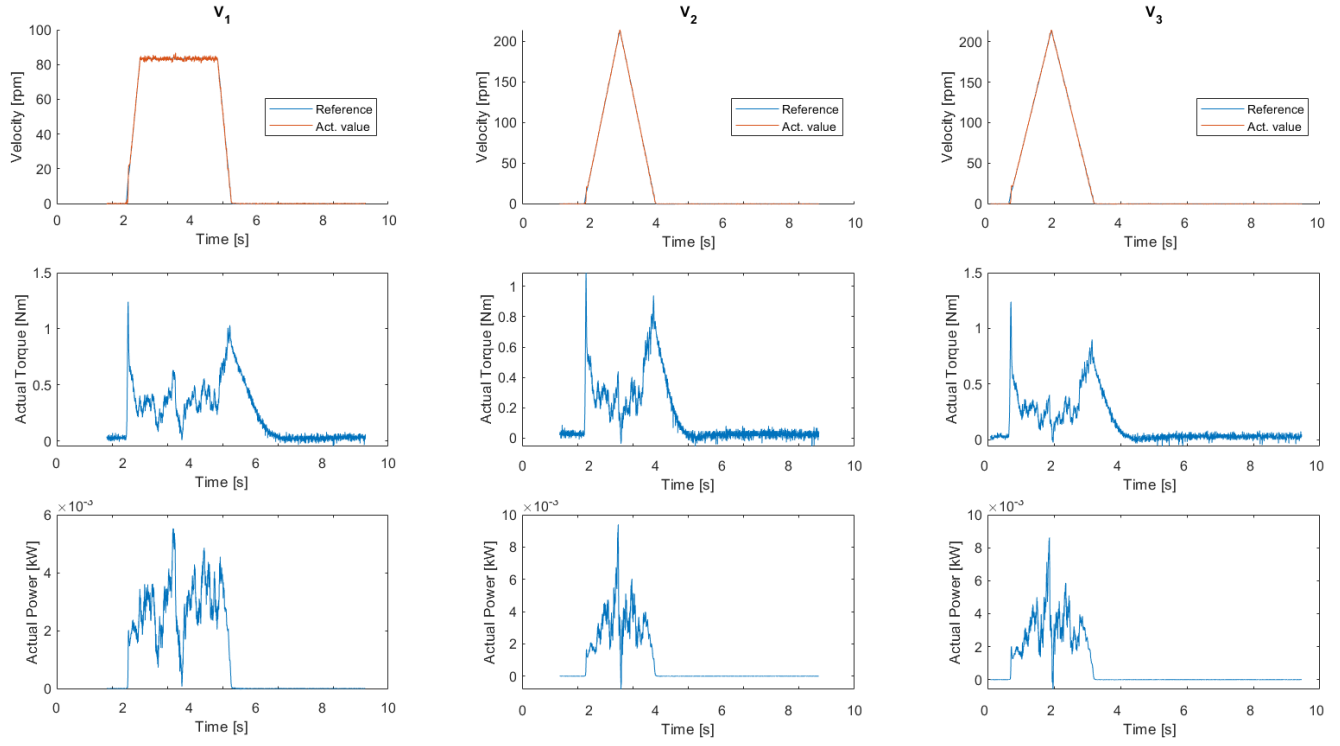

Fig. 10. Test 1. Platform unloaded – movement 250 to 10 mm [source: authors]

The second series of tests consisted of a modified assumption that was tested in the first approach. This time, the movement of the real platform was performed from a level of 10 mm to 250 mm, but with a load of 40.3 kg. The same set of variable values $\phi = 0$ rad and $\vartheta = 0$ rad was assumed again. The approach of selecting inverter settings according to different velocities V

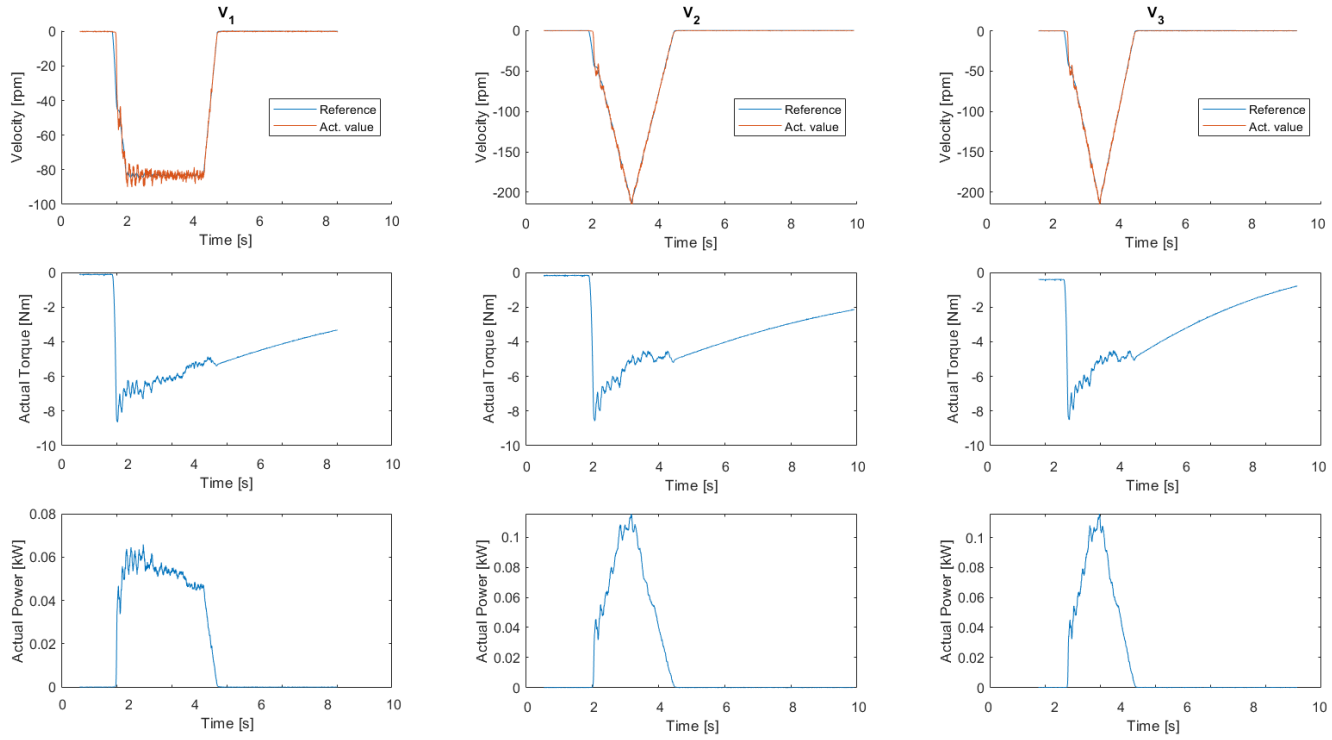

Fig. 11. Test 2. Platform loaded – movement 10 to 250 mm [source: authors]

was used again, where $V_1 < V_2 < V_3$. For each of them, as in the case of the first set of tests, the velocity [rpm], the actual torque [Nm] as well as the actual power [kW] were measured. Measurement charts for this stage are included in Fig. 11 and supported by numerical results using integral quality indicators in Table 4.

The second part of this stage consists of measurements of the loaded Stewart platform from 250 mm to 10 mm. The weight of the load remains constant. An analogous approach was used as in the second part of the first set of tests, when the platform was unloaded. Figure 12 and Table 5 contain the results of these tests.

The third series of the tests has also been important, as it forms a thorough modification of the two previous approaches. In this case, the movement of the real platform was made from a level of 10 mm to 250 mm with a load of 40.3 kg. However, what is very important, this time the values of the ϕ and ϑ variables have been completely modified. In the case of the third series of tests, which includes the 5th and 6th set of tests, the values of these variables were modified as follows: $\phi = -0.043633$ rad, $\vartheta = 0.043633$ rad. This decision is not accidental. At the same time, it allows the research team to assess how, if at all, the measurements of velocity [rpm], actual torque [Nm], as well as actual power [kW] will change. In addition to modifying the values of the mentioned variables, the velocities V will be constantly changed as the set value to the inverter, where $V_1 < V_2 < V_3$. Measurement charts for this stage are included in Fig. 13. The results based on the quality indicators are in Table 6. As in the case of previous tests, the return movement properties of the platform from 250 mm to 10 mm will also be checked. This is a procedure needed to maintain consistency and credibility, and above all, reliability of the research conducted on the object. The load weight is still 40.3 kg. Figure 14 and Table 7 present the results of these tests graphically and numerically.

Table 2
Test result of study 1 (see Fig. 9)

	V_1	V_2	V_3
ISE	5.277×10^3	5.056×10^3	5.146×10^3
MOE	6.955×10^3	4.77×10^3	4.654×10^3
MOE	0.397	0.651	0.643

Table 3
Test result of study 2 (see Fig. 10)

	V_1	V_2	V_3
ISE	1.613×10^3	1.276×10^3	1.426×10^3
MOE	266.656	140.484	131.453
MOE	0.008	0.007	0.007

In order to rationally evaluate the research, it is very important to compare the numerical values generated by tests using selected quality indicators (see Section 5).

So Tables 2–7 contain a comprehensive set of all quality indicator results for 3 test sets covering 6 different tests.

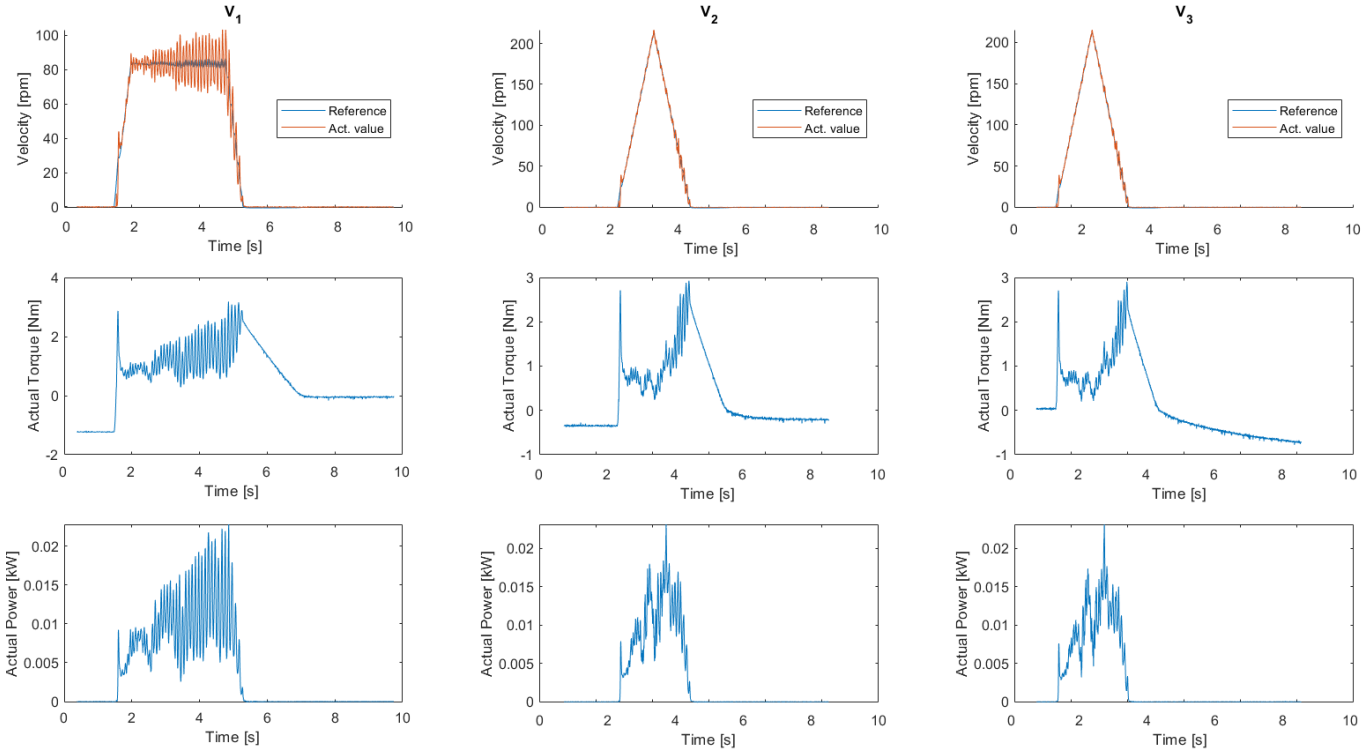

Fig. 12. Test 2. Platform loaded – movement 250 to 10 mm [source: authors]

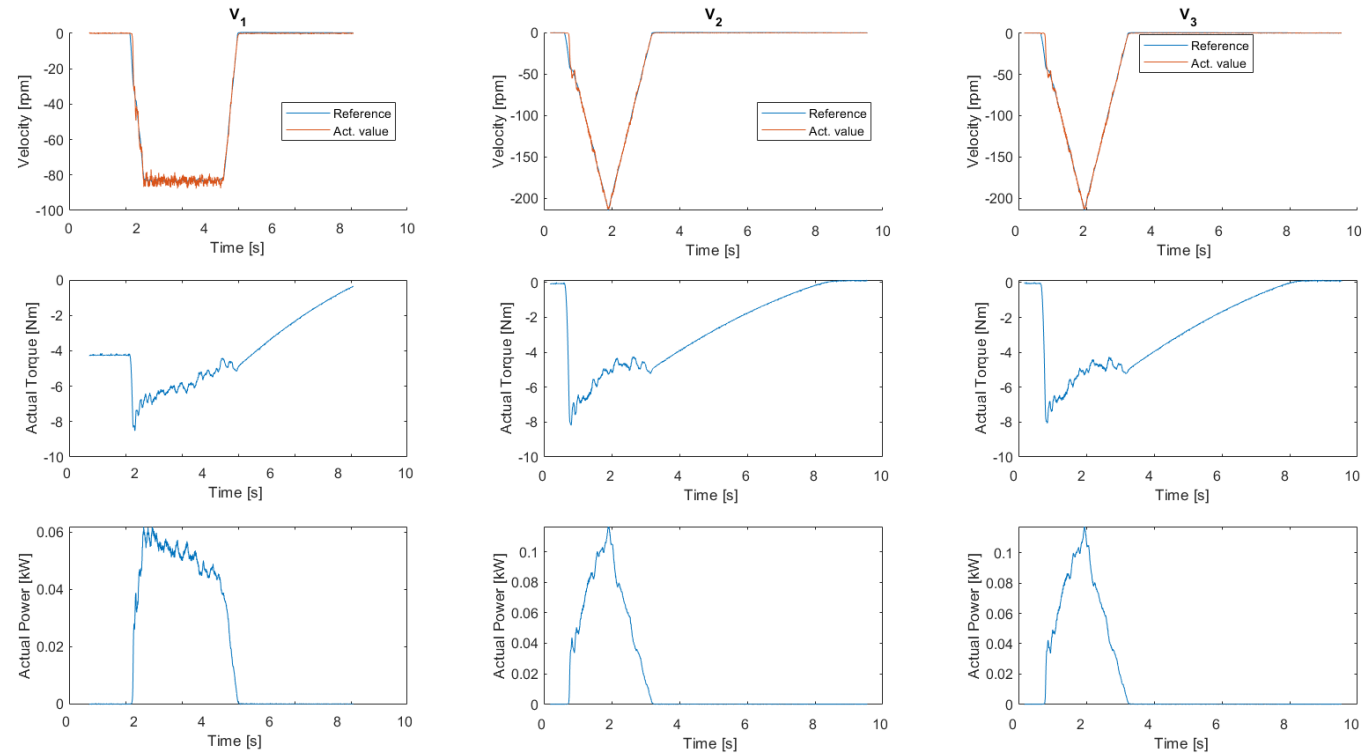

Fig. 13. Test 3. Platform loaded – movement 10 to 250 mm ($\phi = -0.043633$ rad, $\vartheta = 0.043633$ rad) [source: authors]

Analyzing Table 2, which concerns the movement of the unloaded platform from a position of 10 mm to 250 mm, and Table 3 with the results for the movement of the system from 250 mm to 10 mm, clear differences can be noticed. For each of the three

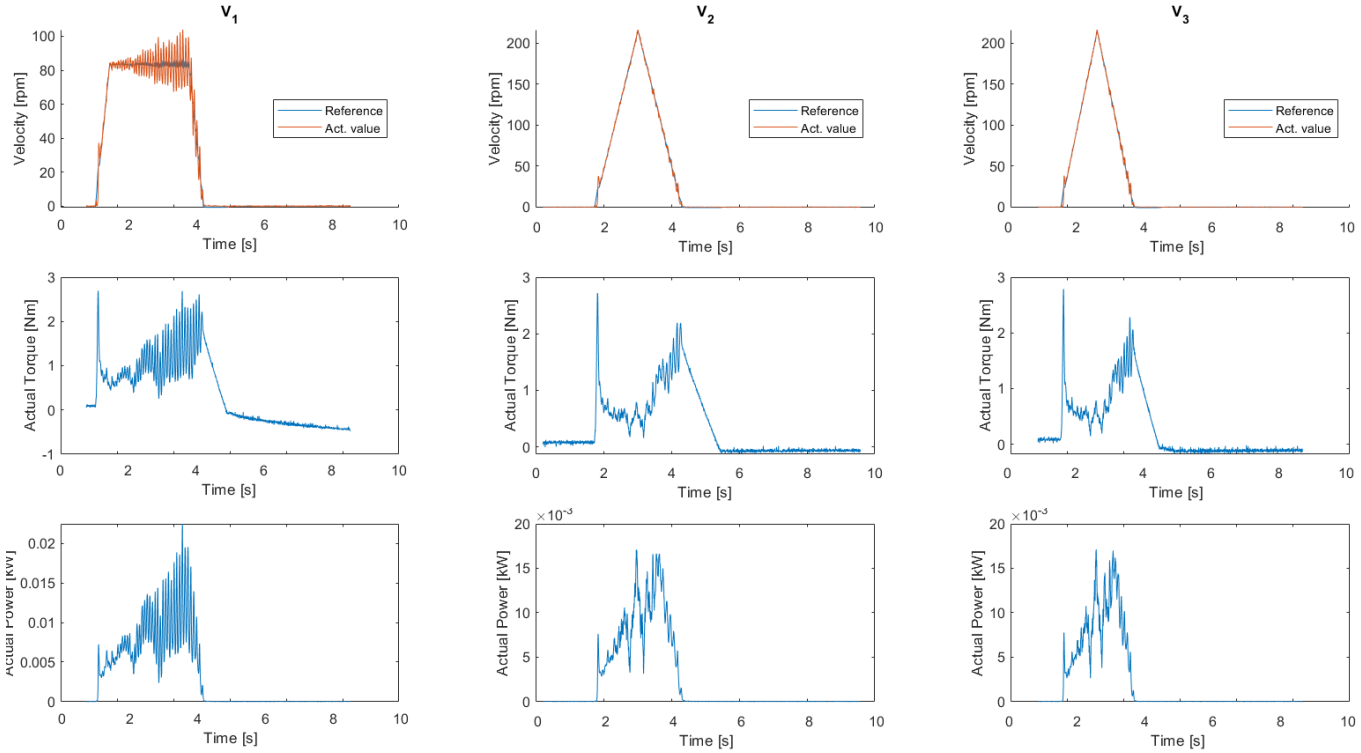

Fig. 14. Test 3. Platform loaded – movement 250 to 10 mm ($\phi = -0.043633$ rad, $\vartheta = 0.043633$ rad) [source: authors]

Table 4
Test result of study 3 (see Fig. 11)

	V_1	V_2	V_3
ISE	2.287×10^4	2.098×10^4	1.949×10^4
MOE	5.547×10^4	3.722×10^4	3.172×10^4
MOE	2.299	3.199	3.171

Table 5
Test result of study 4 (see Fig. 12)

	V_1	V_2	V_3
ISE	7.194×10^4	1.469×10^4	1.203×10^4
MOE	3.262×10^3	1.637×10^3	1.644×10^3
MOE	0.103	0.072	0.065

Table 6
Test result of study 5 (see Fig. 13)

	V_1	V_2	V_3
ISE	8.977×10^3	1.884×10^4	1.843×10^3
MOE	4.848×10^4	2.79×10^4	2.761×10^4
MOE	2.141	3.034	3.043

different velocities as references to the inverter ($V_1 < V_2 < V_3$), the results are significantly different. In the case of the first study,

Table 7
Test result of study 6 (see Fig. 14)

	V_1	V_2	V_3
ISE	4.546×10^3	8.050×10^3	9.005×10^3
MOE	1.702×10^3	0.955×10^3	0.864×10^3
MOE	0.074	0.052	0.051

all values of the ISE indicator (measured velocity value compared with the reference value) have a higher value than in the case of the second approach. There is a very clear difference in the MOE energy index for torque. It is several orders higher in the first test. The situation is similar in the case of the third indicator, which concerns power. Here the situation is analogous to the previous one and a significant difference in values becomes visible. These results were to be expected.

Another very important element of the tests is the second set of tests. They consist of the third and fourth tests. They are included in Tables 4 and 5. The movements of the platform subjected to a load of 40.3 kg from a position of 10 mm to 250 mm, as well as the movements of the system from 250 mm to 10 mm, were analyzed. Similarly to the previously described case, here you can also see different results for each of the three different velocities as set values to the inverter ($V_1 < V_2 < V_3$). However, they are no longer as clear as before. Without a doubt, the load on the platform influenced the obtained measurements. Therefore, the ISE indicator (measured velocity value compared with the reference value) from Tables 4 and 5 is much more similar

to each other than in the case of Tables 2 and 3. However, the results change significantly for the measurement of the MOE indicator related to torque. In the case of movement from a position of 10 mm to 250 mm, a significantly lower energy index result was observed. A similar situation occurs in the case of the third MOE indicator. Here, as in the previous set of unloaded tests, the movement to the original position resulted in a lower value of the integral index. This situation could have been predicted. To summarize the second set of tests, it is possible to observe the difference between the measurements with the platform loaded and without it. However, the trend for each physical quantity was preserved to some extent.

Modification of the variables $\phi = -0.043633$ rad and $\vartheta = 0.043633$ rad did not bring many changes in the context of the research. Studies 5 and 6 for the third test are included in Tables 6 and 7. Here again the trends of the two previous sets of tests, i.e. the four previous studies, are repeated. The results are similar to those in Tables 4 and 5, but are not always consistent. This is especially visible in the example of Table 7. In this case, the value of the ISE index is lower for test 6. For the second and third energy index, i.e. MOE, the results from Table 7 are lower than the corresponding results from Table 5. The results for the set 6 are slightly lower than those for the set of quality indicators 4.

7. CONCLUSIONS

In this manuscript, we have provided a reminder of the design of a functional Stewart real platform with three degrees of freedom. The dynamic nonlinear model developed and partially tested in previous studies [1] is validated in this paper through extensive tests to assess the feasibility of the system. These studies are valuable because they have a practical aspect supported by measurements that applied a real object.

Thanks to its solid metal frame and highly precise drive systems, this platform proves to be an invaluable asset not only in the area of industrial automation, but also in the field of precision robotics. For example, it can significantly expand the range of motion of industrial manipulators, thus opening up new possibilities in the areas of automation and precision tasks. Its usefulness is proven by the fact that the popular company Siemens was interested in the construction.

This type of research allows us to better understand the movement, capabilities and principles of operation of this type of complex robotic devices. As a result of the measurements otbtained as part of the research in this paper, more is known about the capabilities of the Stewart platform. Especially in terms of values such as velocity, torque and power. We also know how the system behaves under various parameters and loads, and how it relates to the reference value.

ACKNOWLEDGEMENTS

The work has been supported by the European Regional Development Fund under the Regional Operational Program of the Opolskie Voivodeship for 2014–2020 for the project entitled 'Research on the development of real-time synchronization technology for electric motors installed in multi-drive industrial elevators', provided by KBA Automatic Sp. z o.o.

REFERENCES

[1] R. Beniak, P. Majewski, M. Witek, Ł. Klar, K. Bochenek, and D. Pawuś, "A high accuracy stewart-lift platform based on a programmable logic controller-theory and practical implementation," *Nonlinear Dyn.*, vol. 112, pp. 1–32, 2024.

[2] Y. Cai, S. Zheng, W. Liu, Z. Qu, J. Zhu, and J. Han, "Adaptive robust dual-loop control scheme of ship-mounted stewart platforms for wave compensation," *Mechan. Mach. Theory*, vol. 164, p. 104406, 2021, doi: 10.1016/j.mechmachtheory.2021.104406.

[3] W.P. Hunek *et al.*, "A measurement-aided control system for stabilization of the real-life stewart platform," *Sensors*, vol. 22, no. 19, p. 7271, 2022, doi: 10.3390/s22197271.

[4] D.-A. Pham, T. N. Pham, and D.-T. Nguyen, "Novel model predictive control-based motion cueing algorithm for compensating centrifugal acceleration in kuka robocoaster-based driving simulators," *Sci. Prog.*, vol. 106, no. 4, p. 00368504231204759, 2023, doi: 10.1177/00368504231204759.

[5] Z.-Q. Lu, D. Wu, H. Ding, and L.-Q. Chen, "Vibration isolation and energy harvesting integrated in a stewart platform with high static and low dynamic stiffness," *Appl. Math. Mod.*, vol. 89, pp. 249–267, 2021, doi: 10.1016/j.apm.2020.07.060.

[6] M. Wang *et al.*, "An adjustable low-frequency vibration isolation stewart platform based on electromagnetic negative stiffness," *Int. J. Mech. Sci.*, vol. 181, p. 105714, 2020.

[7] F. Hu and X. Jing, "A 6-dof passive vibration isolator based on stewart structure with x-shaped legs," *Nonlinear Dyn.*, vol. 91, pp. 157–185, 2018.

[8] H. Yun, L. Liu, Q. Li, W. Li, and L. Tang, "Development of an isotropic stewart platform for telescope secondary mirror," *Mech. Syst. Signal Process.*, vol. 127, pp. 328–344, 2019.

[9] M. Ghosh and S. Dasmahapatra, "Kinematic modeling of stewart platform," in *Intelligent Techniques and Applications in Science and Technology: Proceedings of the First International Conference on Innovations in Modern Science and Technology vol. 1*. Springer, 2020, pp. 693–701.

[10] W. Qiu, S. Wang, A. Niu, K. Fan, G. Han, and H. Chen, "Modeling and analysis of landing collision dynamics for an active helideck based on the stewart platform," *Ocean Eng.*, vol. 297, p. 117107, 2024.

[11] S. N. Nabavi, A. Akbarzadeh, and J. Enferadi, "Closed-form dynamic formulation of a general 6-p us robot," *J. Intell. Robot. Syst.*, vol. 96, pp. 317–330, 2019.

[12] X. Yang, H. Wu, B. Chen, S. Kang, and S. Cheng, "Dynamic modeling and decoupled control of a flexible stewart platform for vibration isolation," *J. Sound Vibr.*, vol. 439, pp. 398–412, 2019, doi: 10.1016/j.jsv.2018.10.007.

[13] T. R. Peterson, "Design and implementation of stewart platform robot for robotics course laboratory," Ph.D. dissertation, California Polytechnic State University, 2020.

[14] T. Zhang, X. Gong, L. Zhang, Y. Wang, Y. Liu, and L. Li, "A method for solving the additional stiffness introduced by flexible joints in stewart platform based on fem modal analysis," *Machines*, vol. 11, no. 4, p. 457, 2023, doi: 10.3390/machines11040457.

[15] F. Tajdari, M. Tajdari, and A. Rezaei, "Discrete time delay feedback control of stewart platform with intelligent optimizer weight tuner," in *2021 IEEE International Conference on Robotics and Automation (ICRA)*, 2021, pp. 12 701–12 707, doi: 10.1109/ICRA48506.2021.9561010.

[16] H. Yadavari, V. Tavakol Aghaei, and S. İkizoğlu, "Deep Reinforcement Learning-Based Control of Stewart Platform With Parametric Simulation in ROS and Gazebo," *J. Mech. Robot.*, vol. 15, no. 3, p. 035001, 2023, doi: 10.1115/1.4056971.

[17] D. Balaban, J. Cooper, and E. Komendera, "Inverse kinematics and sensitivity minimization of an n-stack stewart platform," in *2019 IEEE/RSJ International Conference on Intelligent Robots and Systems (IROS)*. IEEE, 2019, pp. 6794–6799.

[18] W. Wei, Z. Xin, H. Li-Li, W. Min, and Z. You-Bo, "Inverse kinematics analysis of 6–dof stewart platform based on homogeneous coordinate transformation," *Ferroelectrics*, vol. 522, no. 1, pp. 108–121, 2018.

[19] G. Hu, X. Li, and X. Yan, "Inverse kinematics model's parameter simulation for stewart platform design of driving simulator," in *Green Intelligent Transportation Systems: Proceedings of the 7th International Conference on Green Intelligent Transportation System and Safety 7*. Springer, 2018, pp. 887–898.

[20] Y. TANG, Y. ZHUANG, L. SHI, and Y. JIA, "Kinematic analysis of a stewart platform based on afsa," *Univ. Politeh. Buchar. Bull. Ser.-Mech. Eng.*, vol. 81, no. 3, pp. 15–26, 2019.

[21] Y. Liang, J. Zhao, S. Yan, X. Cai, Y. Xing, and A. Schmidt, "Kinematics of stewart platform explains three-dimensional movement of honeybee's abdominal structure," *J. Insect Sci.*, vol. 19, no. 3, p. 4, 2019.

[22] T. Miunske, J. Pradipta, and O. Sawodny, "Model predictive motion cueing algorithm for an overdetermined stewart platform," *J. Dyn. Syst. Measu. Control*, vol. 141, no. 2, p. 021006, 2019.

[23] A. Hameed, A.S.S. Abadi, and A. Ordys, "Model predictive control based motion cueing algorithm for driving simulator," *J. Syst. Sci. Syst. Eng.*, pp. 1–20, 2023, doi: 10.1007/s11518-023-5584-6.

[24] H. Asadi, T. Bellmann, M.C. Qazani, S. Mohamed, C.P. Lim, and S. Nahavandi, "A novel decoupled model predictive control-based motion cueing algorithm for driving simulators," *IEEE Trans. Veh. Technol.*, vol. 72, no. 6, pp. 7024–7034, 2023.

[25] X. Yang, H. Wu, B. Chen, S. Kang, and S. Cheng, "Dynamic modeling and decoupled control of a flexible stewart platform for vibration isolation," *J. Sound Vibr.*, vol. 439, pp. 398–412, 2019.

[26] J. Jiao, Y. Wu, K. Yu, and R. Zhao, "Dynamic modeling and experimental analyses of stewart platform with flexible hinges," *J. Vibr. Control*, vol. 25, no. 1, pp. 151–171, 2019.

[27] Z. Liu, C. Cai, M. Yang, and Y. Zhang, "Testing of a mems dynamic inclinometer using the stewart platform," *Sensors*, vol. 19, no. 19, p. 4233, 2019.

[28] R. Beniak, "Influence of frequency decision taking and torque hysteresis on accuracy of trajectory in industrial manipulator with direct torque control of induction motor drives," *Stud. Appl. Electromagn. Mech.*, vol. 33, p. 459, 2010.

[29] R. Szczepanski, T. Tarczewski, and L. Grzesiak, "PMSM drive with adaptive state feedback speed controller," *Bull. Pol. Acad. Sci. Tech. Sci.*, vol. 68, no. 5, pp. 1009–1017, 2020, doi: 10.24425/bpasts.2020.134624.

[30] D. Pawuś and S. Paszkiel, "Identification and expert approach to controlling the cement grinding process using artificial neural networks and other non-linear models," *IEEE Access*, vol. 12, pp. 26 364–26 383, 2024.

[31] P. Burzynski, A. Simha, Ü. Kotta, E. Pawluszewicz, and S. Sastry, "Flhex: a flapped-paddle hexapod for all-terrain amphibious locomotion," *Bull. Pol. Acad. Sci. Tech. Sci.*, vol. 69, p. e139007, 2021, doi: 10.24425/bpasts.2021.139007.

[32] D. Pawuś and S. Paszkiel, "Application of eeg signals integration to proprietary classification algorithms in the implementation of mobile robot control with the use of motor imagery supported by emg measurements," *Appl. Sci.*, vol. 12, no. 11, p. 5762, 2022, doi: 10.3390/app12115762.

[33] S. Sokół, D. Pawuś, P. Majewski, and M. Krok, "The study of the effectiveness of advanced algorithms for learning neural networks based on fpga in the musical notation classification task," *Appl. Sci.*, vol. 12, no. 19, p. 9829, 2022, doi: 10.3390/app12199829.

[34] T. Kornuta, C. Zieliński, and T. Winiarski, "A universal architectural pattern and specification method for robot control system design," *Bull. Pol. Acad. Sci. Tech. Sci.*, vol. 68, no. 1, pp. 3–29, 2020.

[35] R. Beniak, "Research on the development of real-time synchronization technology for electric motors installed in multi-drive industrial elevators (in Polish)," KBA Automatic Sp. z o.o., Tech. Rep., 2020.

[36] KBA Automatic Sp. z o.o., "Stewart platform - high accuracy elevator," 2023. [Online]. Available: https://www.siemens.com/pl/pl/o-firmie/case-study/platforma-stewarta-winda-duzej-dokladnosci.html

[37] P. Majewski, W. P. Hunek, D. Pawuś, K. Szurpicki, and T. Wojtala, "A sensor-aided system for physical perfect control applications in the continuous-time domain," *Sensors*, vol. 23, no. 4, p. 1947, 2023.